**RESEARCH ARTICLE**

# Single-Layer, Dual-Band, Circularly Polarized, Proximity-Fed Meshed Patch Antenna

**VAN LINH PHAM[1], SON XUAT TA[1],**
**KHAC KIEM NGUYEN[1], (Member, IEEE),**
**CHIEN DAO-NGOC[1], (Senior Member, IEEE),**
**AND NGHIA NGUYEN-TRONG[2], (Member, IEEE)**

[1]School of Electrical and Electronic Engineering, Hanoi University of Science and Technology, Hanoi 100000, Vietnam
[2]School of Electrical and Electronic Engineering, The University of Adelaide, Adelaide, SA 5005, Australia

Corresponding author: Son Xuat Ta (xuat.tason@hust.edu.vn)

**ABSTRACT** This paper proposes a new method to design a single-layer dual-band circularly polarized (CP) patch antenna with a small frequency ratio. The design consists of one or several pairs of rectangular patches proximity-fed by a 50-$\Omega$ microstrip line with an open-circuit termination. By exploiting both capacitive and inductive coupling mechanisms, and both orthogonal radiating modes of these patches, the antenna can be designed to operate at two close resonance frequencies. Due to its simple and single-layer structure, the antenna can be easily adapted with meshed configuration, which is suitable for transparent devices. For verification, a dual-band CP meshed patch antenna with a frequency ratio of 1.12 and two pairs of patch is designed, fabricated, and tested. The measurements show that the antenna prototype provides a $|S_{11}| < -10$-dB bandwidth of $4.82-5.03$ GHz (210 MHz) and $5.49-5.78$ GHz (290 MHz), axial ratio $< 3$-dB bandwidth of $4.88-4.93$ GHz (50 MHz) and $5.50-5.57$ GHz (70 MHz), and broadside realized gains of 9.0 dBic and 8.6 dBic for the lower and upper bands, respectively.

**INDEX TERMS** Single layer, rectangular patch, proximity feed, dual-band, circular polarization, meshed patch.

## I. INTRODUCTION

In recent years, meshed antennas have been received significantly pervasive attention as one a major class for optically transparent antennas [1], [2], [3]. Indeed, meshed configuration is used for almost 50% of the transparent antennas in the literature [2]. Due to their increasing number of applications, such as, integration with solar-cells, wireless sensors, onboard CubeSats or SmallSats, RF identification, broadcast, global positioning systems, 5G, and smart devices, significant efforts have been invested in antenna structures that can be adapted to meshed configuration. Inheriting features of the microstrip antennas [4], including low-profile, lightweight, low cost, and conformability to a shaped surface, the meshed patch antennas [5], [6], [7], [8], [9], [10], [11], [12], [13] are one of the most preferred choices for integration with

solar cells. Nevertheless, the performance of most of these antennas are still limited with single-band operation.

Along with the higher demands in quality of service, data-rate and reliability, many modern wireless communication systems employ different frequency bands. Moreover, some of these systems favorably employ circularly polarized (CP) antennas [14] to mitigate multipath interference, polarization mismatch, and Faraday's effects. Thus, there has been a demand on multi-band CP antennas, which, in some cases, are more reliable than the broadband antennas due to the reduction of out-of-band interference. Furthermore, broadband CP antennas typically require a higher profile or larger planar size. A common approach for designing dual-band CP antennas is to use dual resonant elements printed on multi-layer substrate, i.e., stacked patch configurations [15], [16], [17], [18], [19], [20]. These designs, however, are not suitable for transparent devices as multi-layer structures would reduce the transparency. Some notable

The associate editor coordinating the review of this manuscript and approving it for publication was Binit Lukose.

techniques to design dual-band single-layer CP radiators include embedding Y and T-shape slots [21], using two different rings [22], [23], embedding metamaterial structures [24], loading open-ended stub [25], series-fed patch leaky-wave antenna [26], and adding non-radiative resonators [27]. Nevertheless, there are several challenges when adapting these techniques for meshed antennas. For example, probe feeds [21], [22], [23], [24], [25] and conducting vias [24] should be avoided for transparent devices. Meshing the resonators in [27] can be difficult due to the small gaps and thin conducting lines. In general, to adapt to the meshed configuration, simple structures are desirable because the mesh could alter the currents on the patch, and consequently, change the radiation mechanisms. For this purpose, [26] can be a good option but this technique requires large space for the antenna.

In this paper, a single-layer dual-band CP meshed patch antenna with a small frequency ratio is presented. The design consists of two pairs of meshed patches, which are fed by an open-ended 50-Ω microstrip-line through proximity coupling. Regarding the theoretical aspect, the proposed technique is unique where both inductive and capacitive couplings are exploited at two different frequencies by the same simple feeding structure. Regarding the practical aspect, the design avoids using probe feed, shorting vias, and any extra non-radiating or radiating element, which makes it suitable for adapating on transparent devices. As a validation, a dual-band CP antenna with a frequency ratio of 1.12 is characterized using the ANSYS Electronics Desktop and validated experimentally.

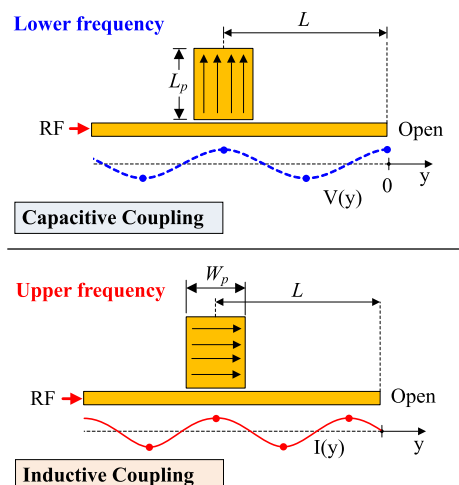## II. RESONANT-TYPE PROXIMITY-FED PATCH ANTENNA

For completion, we first present the theory of a resonant-type proximity-fed patch antenna. The proximity-fed method was first presented by Itoh and Ohtsuka in 1982 [28] to avoid the multi-layer structure and exploit the advantages of non-contacting coupling feeds. It should be noted the principle is different from the traveling-wave structures as in [26], [29], and [30].

The basic structure is shown in Fig. 1, which consists of a rectangular patch fed from a microstrip line with distance $L$ from its open-circuit termination. This creates a standing-wave on the microstrip line with maximum voltage and zero current at the termination. Interestingly, two types of coupling occur in this structure at two different frequencies:
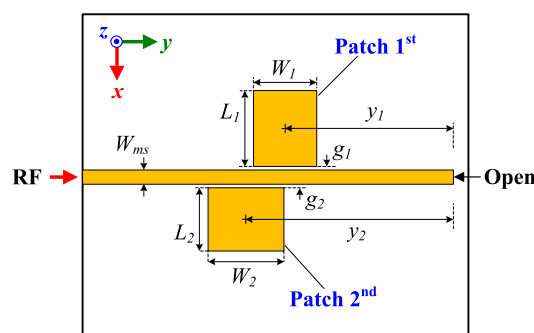
1) At a frequency $f_1$ with guided-wavelength $\lambda_{g1}$, if

$$L = \frac{n\lambda_{g1}}{2}, \qquad (1)$$

where $n$ is an integer, the patch is aligned at $V_{\max}$. If the patch length $L_p \approx \lambda_{\mathrm{eff1}}/2$, the patch resonates at $TM_{10}$ mode with vertical polarization through capacitive coupling. It is noted that $\lambda_{g1} \neq \lambda_{\mathrm{eff1}}$ as the effective permittivities of the patch and the microstrip line are different.



**FIGURE 1.** Coupling mechanisms of coplanar proximity feed for a rectangular patch at different frequencies.



**FIGURE 2.** Top-view of the proposed dual-band CP proximity-fed patch antenna with one pair of patch.

2) At a different frequency $f_2$ with guided-wavelength $\lambda_{g2}$, if

$$L = \frac{n\lambda_{g2}}{2} + \frac{\lambda_{g2}}{4}, \qquad (2)$$

where $n$ is also an integer, the patch is aligned with $I_{\max}$. If the patch width $W_p \approx \lambda_{\mathrm{eff2}}/2$, the patch resonates in $TM_{01}$ mode with horizontal polarization through inductive coupling.

Therefore, the structure works as a dual-band linear-polarized (LP) antenna where the polarization in each band is orthogonal to each other. Furthermore, the level of coupling, which affects the impedance matching, can be controlled by the gap between the patches and the feed lines. The principle demonstrated here is a generalization of what shown in [7], which will be exploited to design a dual-band CP antenna in the next section.

## III. DUAL-BAND CP PROXIMITY-FED PATCH ANTENNA
### A. PRINCIPLE AND DESIGN

A CP antenna can be realized if a vertically polarized patch and a horizontally polarized patch are both excited with 90° phase difference. Since the standing-wave current and voltage

**TABLE 1.** Parameters of dual-band CP patch antenna.

| Par. | Value (mm) | Par. | Value (mm) | Par. | Value (mm) |
|------|-----------|------|-----------|------|-----------|
| $W_1$ | 13.2 | $L_1$ | 15.2 | $W_2$ | 15.35 |
| $L_2$ | 13.2 | $y_1$ | 37 | $y_2$ | 45 |
| $g_1$ | 0.4 | $g_2$ | 0.4 | $W_{ms}$ | 3.6 |



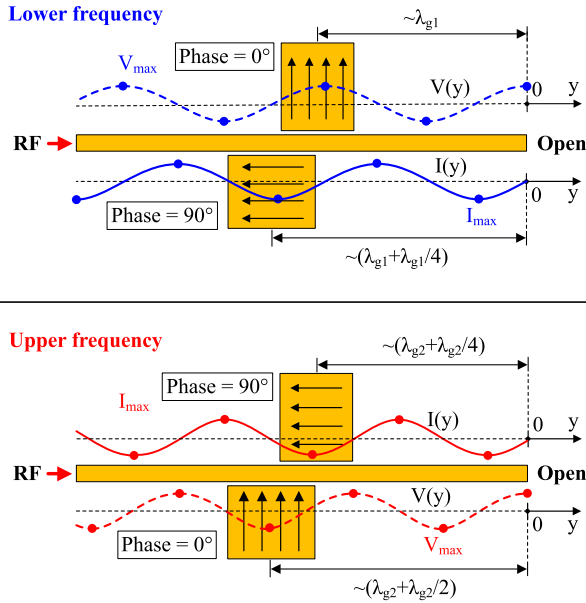**FIGURE 3.** Capacitive and inductive coupling mechanisms of microstrip-line feed for the patches at two different frequencies.



**FIGURE 4.** Current distribution on the dual-band CP patch antenna for different phases: (a) lower frequency of 5.0 GHz and (b) upper frequency of 5.6 GHz.

are inherently 90° phase different, this is naturally achieved and will be exploited in the design.

Fig. 2 shows the geometry of the proposed concept, which consists of a pair of patch fed by an open-ended 50-Ω microstrip-line through proximity coupling. The two patches and feedline are printed on the top side of a single-layer grounded substrate (Roger RO4003, $\epsilon_r = 3.55$, $\tan \delta = 0.0021$, $h_s = 1.524$ mm). To operate at two different frequencies, $f_1$ and $f_2$, the length and width of each patch are chosen as about $\lambda_{\text{eff1}}/2$ and $\lambda_{\text{eff2}}/2$, respectively.

According to the principle demonstrated in Section II, we select the position of the patches from the open termination such that

$$y_1 \approx \begin{cases} n\lambda_{g1}/2 & \text{at } f_1 \\ n\lambda_{g2}/2 + \lambda_{g2}/4 & \text{at } f_2 \end{cases} \quad (3)$$

and

$$y_2 \approx \begin{cases} n\lambda_{g1}/2 + \lambda_{g1}/4 & \text{at } f_1 \\ (n+1)\lambda_{g2}/2 & \text{at } f_2 \end{cases} \quad (4)$$

where $n$ is an integer. If (3) and (4) are satisfied, at $f_1$, the 1st patch (Fig. 2) resonates at $TM_{10}$ mode while the 2nd patch resonates at $TM_{01}$ mode. Meanwhile, at $f_2$, the 1st patches resonate at $TM_{01}$ mode and the 2nd patch resonates at $TM_{10}$ mode.
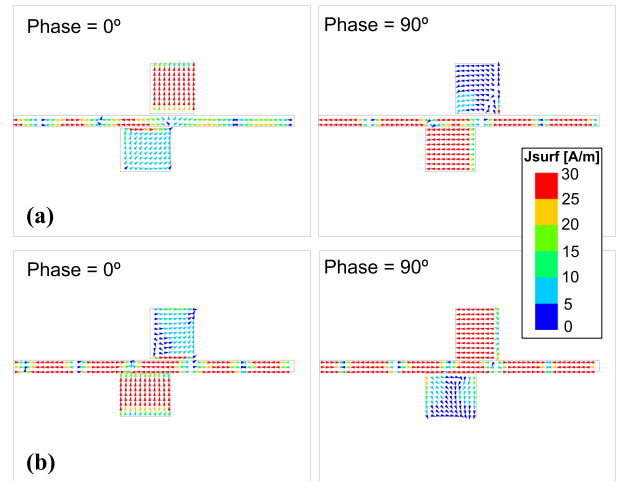
Finally, as mentioned before, the standing-wave voltage and current have 90° phase difference, thus, CP radiation at both resonance frequencies can be achieved. Fig. 3 illustrates the standing-wave voltage and current along the microstrip line, and how CP is achieved at both lower and upper bands. By tuning the patch dimensions as well as the positions $y_1$ and $y_2$, it will be shown later that satisfactory axial ratio (AR) and broadside radiation can still be achieved.

For demonstration, a design with a frequency ratio of 1.12 (operating at 5.0 GHz and 5.6 GHz) is characterized. Its design parameters are given in Table 1. The simulation results will be shown in the next section. To confirm the analysis shown in Fig. 3, the surface currents on the antenna are simulated at the two frequencies of 5.0 GHz and 5.6 GHz and given in Fig. 4. For the lower frequency, at 0° phase, the dominant currents on the 1st patch are vertical ($TM_{10}$ mode), whereas at 90° phase, the dominant currents on the 2nd patch are in horizontal direction ($TM_{01}$ mode). For the upper frequency, at 0° phase, the dominant currents on the 1st patch are horizontal, whereas at 90° phase, the dominant currents on the 2nd patch are vertical. These simulation results are consistent with the above analysis. It can be confirmed from Fig. 4 that the antenna achieves a right-hand CP (RHCP) radiation at both frequencies. By simply mirroring the patches through the feed-line, the proposed antenna achieves a dual-band left-hand CP (LHCP) radiation.

### B. DIFFERENT NUMBERS OF PATCH
Based on the proposed method, dual-band CP antennas with gain enhancement can be realized by adding more radiating elements, as shown in Fig. 5. For the second and third pairs of patches, it needs to resonate with the same phase as the first pair. Strictly speaking, this cannot be satisfied at both frequencies $f_1$ and $f_2$ at the same time. However, a compromise can be made when $f_1$ and $f_2$ are very close to each other (so that $\lambda_{g2}$ is close to $\lambda_{g1}$). Here we can choose $y_3 \approx y_4 \approx 0.5(\lambda_{g2} + \lambda_{g1})$. After the optimization, $y_3 = 33.8$ mm and
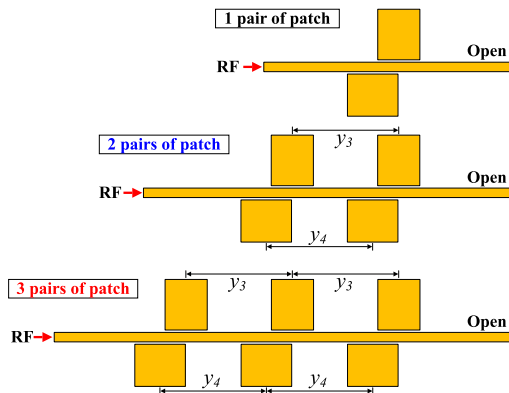
**FIGURE 5.** Geometry of the dual-band CP patch antenna with different number of patch.
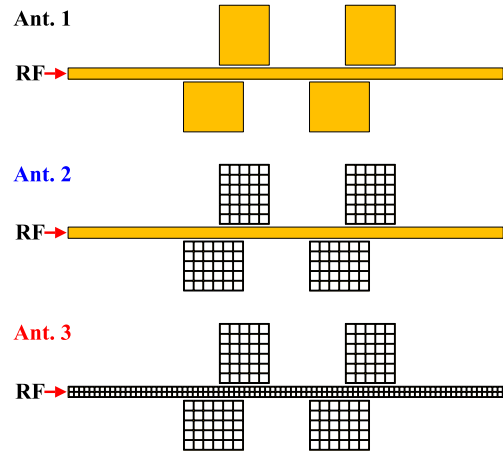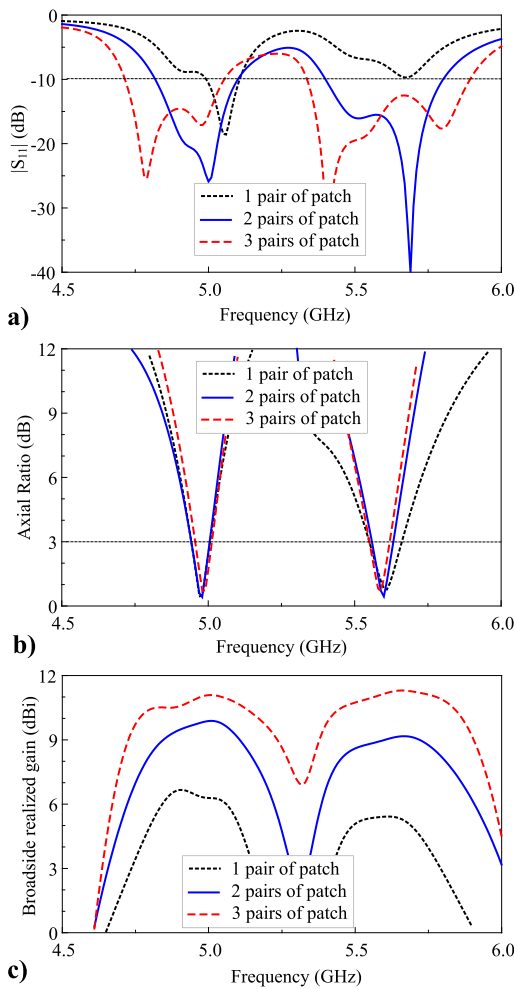


**FIGURE 6.** Simulated performances of the dual-band CP patch antenna for different numbers of patch: (a) $|S_{11}|$, (b) axial ratio, and (c) broadside realized gain.

$y_4 = 33.4$ mm are chosen for both designs with the double and triple pairs of patch, while their other parameters are same as those listed in Table 1.

All antennas in Fig. 5 are characterized and their performances are compared in Fig. 6. It is observed that the three



**FIGURE 7.** Different configurations of the dual-band CP patch antenna.

configurations achieve good CP radiations at dual frequency. As the number of patches increases, the impedance matching, bandwidth, and gain are improved for both lower and upper bands [Figs. 6(a) and (c)]. The antenna with a single pair of patch does not yield satisfactory impedance matching, which is due to the slightly weak coupling between the patches and the feed line. By adding more patchs, the coupling is enhanced, and consequently, the impedance matching in the antennas with double and triple pairs of patch is improved [Fig. 6(a)]. Due to the same CP radiation mechanism, their AR characteristics are nearly identical, as shown in Fig. 6(b). From Fig. 6(c), the broadside gains at both frequency-bands are proportionally increased by adding more number of patches; i.e., the single pair of patch antenna yields gain of 6.5 and 5.9 dBi at 5.0 and 5.6 GHz, respectively, while the gains at both bands increase $\sim$3 dB and $\sim$4.8 dB for the double and triple pair of patch designs, respectively.

## IV. DUAL-BAND CP MESHED PATCH ANTENNAS
### A. DIFFERENT MESHED CONFIGURATIONS
Due its simplicity, the proposed concept is well suited for transparent antennas, as also illustrated with a single-band CP antenna in [7]. For demonstration, dual-band CP antennas with two pairs of patches are implemented, as shown in Fig. 7. Ant. 1 is the dual-band CP antenna with double pair of solid-patch, while the patches of other designs are meshed. For the Ants. 2 and 3, each patch is meshed into $6 \times 5$ meshes with a line width of 0.2 mm. For Ant. 3, the feed-line is meshed; i.e. its width is meshed into 2-cells with a line width of 0.2 mm. Although an optically transparent dielectric (e.g., glass or polymer) is required for an actual transparent antenna, the design philosophy is the same for transparent and non-transparent substrates. Thus, the Roger's RO4003C laminate ($\epsilon_r = 3.55$, $\tan \delta = 0.0021$, and $h_s = 1.524$ mm) is chosen for the validation of the proposed method. Since the mesh changes the sheet resistance of the patch, the design parameters of the meshed patch antennas are slightly
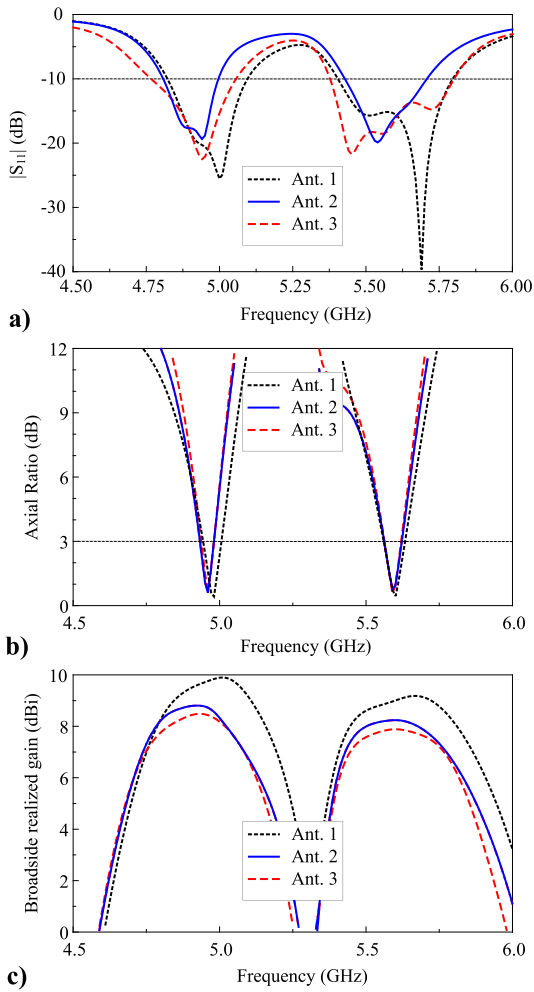
**FIGURE 8.** Performance comparison of the different antennas: (a) $|S_{11}|$, (b) axial ratio, and (c) broadside realized gain.

**TABLE 2.** Parameters of dual-band CP meshed patch prototype.

| Par. | Value (mm) | Par. | Value (mm) | Par. | Value (mm) |
|------|-----------|------|-----------|------|-----------|
| $W_1$ | 12.45 | $L_1$ | 14.1 | $W_2$ | 14.4 |
| $L_2$ | 12.25 | $W_3$ | 12.45 | $L_3$ | 14.1 |
| $W_4$ | 14.4 | $L_4$ | 12.25 | $g$ | 0.4 |
| $y_1$ | 37 | $y_2$ | 45 | $y_3$ | 33.4 |
| $y_4$ | 33.8 | $W_{ms}$ | 3.6 | $h_s$ | 1.524 |

modified as compared to the solid patch. Referring to Figs. 2 and 5, the optimized parameters of Ants. 2 and 3 are given in Table 2.

The three different configurations in Fig. 7 are characterized as demonstrated in Fig. 8. The three antennas achieve a good dual-band CP radiation; i.e., good impedance matching, AR values <1 dB at 5.0 and 5.6 GHz, and broadside gains of >8.0 dBic. As shown in Figs. 8(a) and (b), the $|S_{11}|$ and AR curves are quite similar for the three configurations. As analyzed in [2], [5], and [6], the conductivity ($\sigma$) of meshed sheet is less than the conductivity of solid-sheet, and consequently, the radiation efficiencies (REs) of the meshed patch antennas
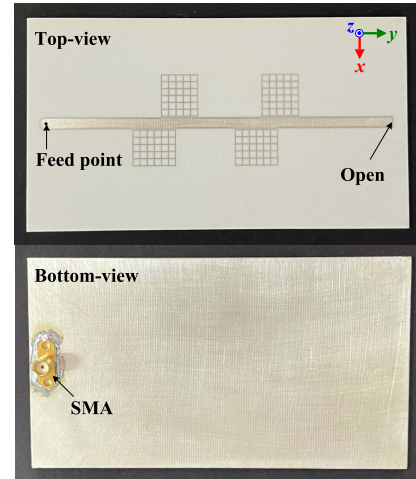


**FIGURE 9.** Fabricated prototype of the dual-band CP meshed patch antenna.

(Ants. 2 and 3) are less than the RE of Ant. 1. Accordingly, the meshed patch antennas yield a lower gain as compared to the solid patch design, as illustrated in Fig. 8(c). With the meshed transmission line, the gain of Ant. 3 shows a drop of about 0.3-dB relative to Ant. 2. The meshed transmission lines have been investigated in [31], [32], [33], and [34], which also showed a minor additional losses (depending on the transparency).

### B. MEASUREMENTS
For verification, the meshed patch antenna with solid feed-line (Ant. 2) is fabricated and tested. It is noted that for applications such as integration with solar cells, thin transmission lines might not be necessary to mesh [7]. Fig. 9 shows a prototype of the fabricated antenna. The antenna is fabricated using the standard printed circuit board technology. The prototype employs a SubMiniature version A (SMA) connector as coaxial-to-microstripline transformer. The simulation and measurement performances of the antenna prototype are compared in Fig. 10. There is a good agreement between the simulated and measured results. From Fig. 10(a), the antenna prototype yields a measured −10-dB impedance bandwidth of 210 MHz/290 MHz (about 4.3% and 5.1% at the lower and upper band, respectively). In Fig. 10(b), the measurements result in a AR bandwidth (AR < 3 dB) of about 50 MHz/70 MHz, i.e. corresponding to 1.0% and 1.3% at the the lower and upper band, respectively. As shown in Fig. 10(c), the fabricated mesh prototype achieves a good broadside gain at both frequency bands, which agrees well with the simulations. The meshed patch antenna yields measured gains of about 9.0 dBic at 4.9 GHz and 8.6 dBic at 5.5 GHz. Finally, simulations of the meshed design indicate radiation efficiencies (RE) of 70% and 76% at the lower and upper bands, respectively. Similar to any meshed antennas in literature, there is a tradeoff between the transparency and radiation efficiency [5]. Although the measured RE is not
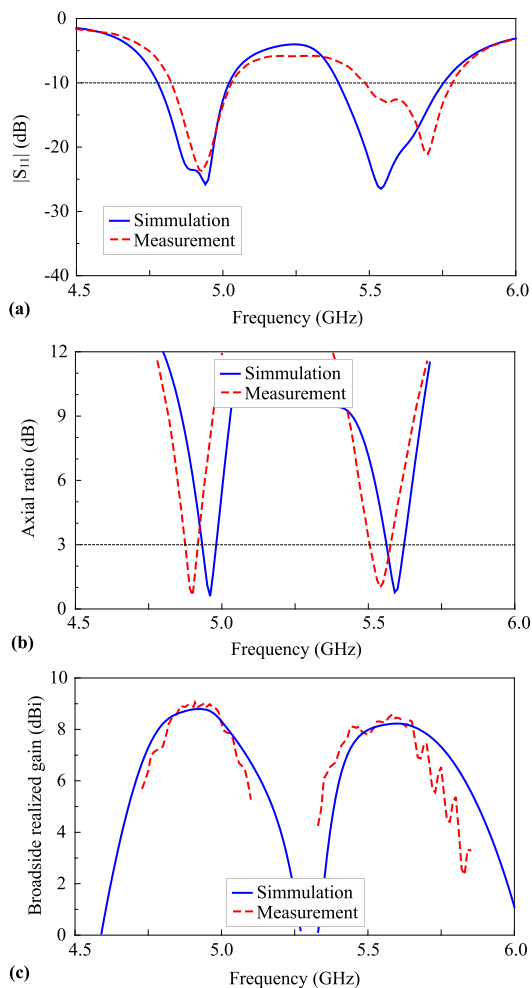
**FIGURE 10.** Simulated and measured (a) $|S_{11}|$; (b) AR values; and (c) realized gain of the dual-band CP meshed patch antenna.



**FIGURE 11.** Radiation patterns of the meshed patch antenna prototype.

**TABLE 3.** A comparison of the proposed antenna and the previous meshed patch antennas.

| Ant. | No. of layers | Bands (GHz) | Pol. | $\mid S_{11}\mid$ BW (%) | AR BW (%) | Gain (dB) |
|---|---|---|---|---|---|---|
| [6] | 1 | Single | LP | 1.2 | - | 1.0 |
| [7] | 1 | Single | CP | 2.0 | 0.6 | 5.15 |
| [8] | 2 | Dual | CP | 2.9/1.5 | 0.85/10.5 | 4.4/4.8 |
| [9] | 2 | Single | CP | 7.25 | 3.27 | 4.4 |
| [10] | 1 | Single | LP | 2.63 | - | 7.2 |
| [11] | 1 | Single | CP | 1.45 | 1.45 | 4.0 |
| [12] | 1 | Single | LP | 6.7 | - | N/A |
| **Prop.** | **1** | **Dual** | **CP** | **4.9/6.5** | **1.04/1.07** | **9.0/8.6** |

CP: Circular polarization, LP: Linear Polarization, N/A: not mentioned

available due to the function limitation of the anechoic chamber, the good agreement between the simulated and measured gains also indicates a similar value of around 70% for the practical RE.

The radiation patterns of the antenna prototype are illustrated in Fig. 11. Note that the simulation and measurement results are plotted for the frequencies where the AR values are at minimum. Observably, at both frequencies, the antenna achieves a good broadside RHCP radiation with reasonably symmetric pattern and high front-to-back ratio. At the broadside, the measured RHCP field intensity is >20 dB larger than that of LHCP for the both bands. At both frequencies, the measurements result in half-power beamwidths of about 72° and 40° in the *xz* and *yz*-plane, respectively.

## C. DISCUSSION

Table 3 shows a comparison between the proposed antenna and previous meshed patch antennas. It is noted that our design exploits the advantage of simple feeding from series-fed patch structure. As illustrated in Table 3, only the
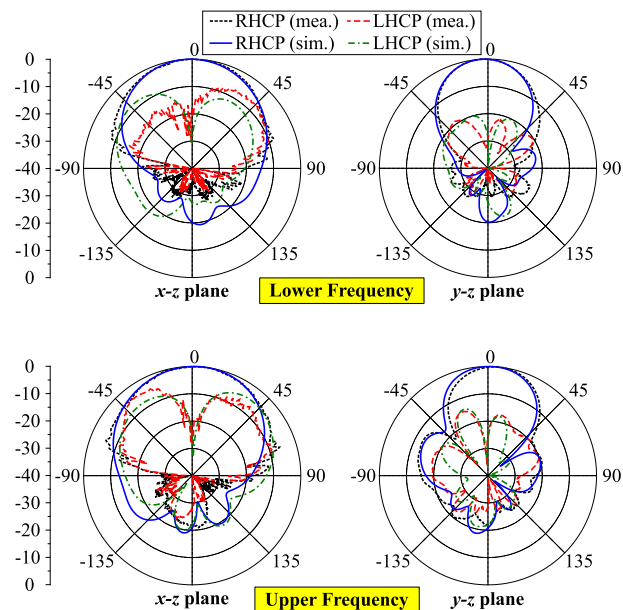
antenna in [8] provides a dual-band CP radiation, however, it uses metamaterial components, which makes it not transparent in a large feeding region. It is also more complicated with multi-layered structure. To achieve higher gain, the antenna in [8] would require more complex feeding network with array configuration, as compared to the proposed design.

## V. CONCLUSION

A method of designing a simple dual-band CP patch antenna with tight frequency ratio has been described. The antenna consists of one/several pair of rectangle patches, which are excited by an open-ended 50-Ω microstrip line through proximity coupling. Based on the capacitive and inductive couplings, the dimensions and arrangement of these patches are designed to generate a dual-band CP radiation. Due to its simplicity, the design is well suited for applications requiring transparent radiators. For demonstration, a dual-band CP meshed patch antenna with a frequency ratio of 1.12 at C-band has been designed, fabricated, and tested. It is emphasized again that although non-transparent substrate has been

used, the theory, design method and procedure are the same for trasparent or non-transparent substrates. The antenna prototype yields a $|S_{11}| < -10$ dB bandwidth of $4.82-5.03$ GHz (210 MHz) and $5.49-5.78$ GHz (290 MHz), AR $< 3$-dB bandwidth of $4.88-4.93$ GHz (50 MHz) and $5.50-5.57$ GHz (70 MHz), and a high measured gain of 9.0 dBic and 8.6 dBic for the lower and upper bands, respectively.

## REFERENCES

[1] T. Yekan and R. Baktur, "Conformal integrated solar panel antennas: Two effective integration methods of antennas with solar cells," *IEEE Antennas Propag. Mag.*, vol. 59, no. 2, pp. 69–78, Apr. 2017.

[2] Z. J. Silva, C. R. Valenta, and G. D. Durgin, "Optically transparent antennas: A survey of transparent microwave conductor performance and applications," *IEEE Antennas Propag. Mag.*, vol. 63, no. 1, pp. 27–39, Feb. 2021.

[3] O. R. Alobaidi, P. Chelvanathan, S. K. Tiong, B. Bais, M. A. Uzzaman, and N. Amin, "Transparent antenna for green communication feature: A systematic review on taxonomy analysis, open challenges, motivations, future directions and recommendations," *IEEE Access*, vol. 10, pp. 12286–12321, 2022.

[4] K.-F. Lee and K.-F. Tong, "Microstrip patch antennas-basic characteristics and some recent advances," *Proc. IEEE*, vol. 100, no. 7, pp. 2169–2180, Jul. 2012.

[5] G. Clasen and R. Langley, "Meshed patch antennas," *IEEE Trans. Antennas Propag.*, vol. 52, no. 6, pp. 1412–1416, Jun. 2004.

[6] T. W. Turpin and R. Baktur, "Meshed patch antennas integrated on solar cells," *IEEE Antennas Wireless Propag. Lett.*, vol. 8, pp. 693–696, 2009.

[7] T. Yasin and R. Baktur, "Circularly polarized meshed patch antenna for small satellite application," *IEEE Antennas Wireless Propag. Lett.*, vol. 12, pp. 1057–1060, 2013.

[8] C. G. M. Ryan and G. V. Eleftheriades, "Single- and dual-band transparent circularly polarized patch antennas with metamaterial loading," *IEEE Antennas Wireless Propag. Lett.*, vol. 14, pp. 470–473, 2015.

[9] S. Sheikh, "Circularly polarized meshed patch antenna," *IEEE Antennas Wireless Propag. Lett.*, vol. 15, pp. 352–355, 2015.

[10] T. Yasin and R. Baktur, "Bandwidth enhancement of meshed patch antennas through proximity coupling," *IEEE Antennas Wireless Propag. Lett.*, vol. 16, pp. 2501–2504, 2017.

[11] S. K. Podilchak, D. Comite, B. K. Montgomery, Y. Li, V. Gomez-Guillamon Buendia, and Y. M. M. Antar, "Solar-panel integrated circularly polarized meshed patch for cubesats and other small satellites," *IEEE Access*, vol. 7, pp. 96560–96566, 2019.

[12] B. Xi, X. Liang, Q. Chen, K. Wang, J. Geng, and R. Jin, "Optical transparent antenna array integrated with solar cell," *IEEE Antennas Wireless Propag. Lett.*, vol. 19, no. 3, pp. 457–461, Mar. 2020.

[13] T. Yekan and R. Baktur, "Study of the impact between a triple junction space solar cell and the antenna integrated on top of it," *IEEE Trans. Antennas Propag.*, vol. 69, no. 3, pp. 1734–1739, Mar. 2020.

[14] S. Gao, Q. Luo, and F. Zhu, *Circularly Polarized Antennas*. New York, NY, USA: Wiley, Nov. 2013.

[15] S. Chen, G. C. Liu, X. Y. Chen, T. Lin, X. Liu, and Z. Duan, "Compact dual-band GPS microstrip antenna using multilayer LTCC substrate," *IEEE Antennas Wireless Propag. Lett.*, vol. 9, pp. 421–423, 2010.

[16] P. Nayeri, K.-F. Lee, A. Z. Elsherbeni, and F. Yang, "Dual-band circularly polarized antennas using stacked patches with asymmetric U-slots," *IEEE Antennas Wireless Propag. Lett.*, vol. 10, pp. 492–495, 2011.

[17] C. Deng, Y. Li, Z. Zhang, G. Pan, and Z. Feng, "Dual-band circularly polarized rotated patch antenna with a parasitic circular patch loading," *IEEE Antennas Wireless Propag. Lett.*, vol. 12, pp. 492–495, 2013.

[18] H.-X. Xu, G.-M. Wang, J.-G. Liang, M. Q. Qi, and X. Gao, "Compact circularly polarized antennas combining meta-surfaces and strong space-filling meta-resonators," *IEEE Trans. Antennas Propag.*, vol. 61, no. 7, pp. 3442–3450, Jul. 2013.

[19] Y. Li, B. Tian, J. Xue, and G. Ge, "Compact dual-band circularly polarized antenna design for navigation terminals," *IEEE Antennas Wireless Propag. Lett.*, vol. 15, pp. 802–805, 2016.

[20] T. Yue, Z. H. Jiang, and D. H. Werner, "A compact metasurface-enabled dual-band dual-circularly polarized antenna loaded with complementary split ring resonators," *IEEE Trans. Antennas Propag.*, vol. 67, no. 2, pp. 794–803, Feb. 2019.

[21] K.-P. Yang and K.-L. Wong, "Dual-band circularly-polarized square microstrip antenna," *IEEE Trans. Antennas Propag.*, vol. 49, no. 3, pp. 377–382, Mar. 2001.

[22] X. L. Bao and M. J. Ammann, "Dual-frequency circularly-polarized patch antenna with compact size and small frequency ratio," *IEEE Trans. Antennas Propag.*, vol. 55, no. 7, pp. 2104–2107, Jul. 2007.

[23] Z.-X. Liang, D.-C. Yang, X.-C. Wei, and E.-P. Li, "Dual-band dual circularly polarized microstrip antenna with two eccentric rings and an arc-shaped conducting strip," *IEEE Antennas Wireless Propag. Lett.*, vol. 15, pp. 834–837, 2016.

[24] S.-T. Ko, B.-C. Park, and J.-H. Lee, "Dual-band circularly polarized patch antenna with first positive and negative modes," *IEEE Antennas Wireless Propag. Lett.*, vol. 12, pp. 1165–1168, 2013.

[25] N.-W. Liu, L. Zhu, Z.-X. Liu, Z.-Y. Zhang, and G. Fu, "Frequency-ratio reduction of a low-profile dual-band dual-circularly polarized patch antenna under triple resonance," *IEEE Antennas Wireless Propag. Lett.*, vol. 19, no. 10, pp. 1689–1693, Oct. 2020.

[26] C. D. Bui, N. Nguyen-Trong, and T. K. Nguyen, "A planar dual-band and dual-sense circularly polarized microstrip patch leaky-wave antenna," *IEEE Antennas Wireless Propag. Lett.*, vol. 19, no. 12, pp. 2162–2166, Dec. 2020.

[27] Q.-S. Wu, X. Zhang, L. Zhu, J. Wang, G. Zhang, and C.-B. Guo, "A single-layer dual-band dual-sense circularly-polarized patch antenna array with small frequency ratio," *IEEE Trans. Antennas Propag.*, vol. 70, no. 4, pp. 2668–2675, Apr. 2022.

[28] K. Itoh and H. Ohtsuka, "New polarization switching technique of microstrip antenna," in *Proc. 12th Eur. Microw. Conf.*, Oct. 1982, pp. 349–354.

[29] S. J. Chen, C. Fumeaux, Y. Monnai, and W. Withayachumnankul, "Dual circularly polarized series-fed microstrip patch array with coplanar proximity coupling," *IEEE Antennas Wireless Propag. Lett.*, vol. 16, pp. 1500–1503, 2017.

[30] N. Nguyen-Trong, S. J. Chen, and C. Fumeaux, "High-gain dual-band dual-sense circularly polarized spiral series-fed patch antenna," *IEEE Open J. Antennas Propag.*, vol. 3, pp. 343–352, 2022.

[31] J. Hautcoeur, L. Talbi, and K. Hettak, "Feasibility study of optically transparent CPW-fed monopole antenna at 60-GHz ISM bands," *IEEE Trans. Antennas Propag.*, vol. 61, no. 4, pp. 1651–1657, Apr. 2013.

[32] J. Hautcoeur, L. Talbi, K. Hettak, and M. Nedil, "60 GHz optically transparent microstrip antenna made of meshed AuGL material," *IET Microw., Antennas Propag.*, vol. 8, no. 13, pp. 1091–1096, Oct. 2014.

[33] E. R. Escobar, N. J. Kirsch, G. Kontopidis, and B. Turner, "5.5 GHz optically transparent mesh wire microstrip patch antenna," *Electron. Lett.*, vol. 51, no. 16, pp. 1220–1222, 2015.

[34] J. Park, S. Y. Lee, J. Kim, D. Park, W. Choi, and W. Hong, "An optically invisible antenna-on-display concept for millimeter-wave 5G cellular devices," *IEEE Trans. Antennas Propag.*, vol. 67, no. 5, pp. 2942–2952, May 2019.

**VAN LINH PHAM** is currently pursuing the B.Sc.(Eng.) degree in electronics and telecommunications with the Hanoi University of Science and Technology (HUST), Vietnam. Since 2020, he has been working as an Internship Researcher at the Communication Research and Development Laboratory, HUST. His research interests include microstrip patch antennas, mesh patch antennas, circularly polarized antennas, and multiband antennas.

**SON XUAT TA** received the B.Sc.(Eng.) degree in electronics and telecommunications from the Hanoi University of Science and Technology, Vietnam, in August 2008, and the Ph.D. degree in electrical engineering from Ajou University, South Korea, in February 2016. From March 2016 to February 2017, he was a Postdoctoral Research Fellow with the Department of Electrical and Computer Engineering, Ajou University. From March 2017 to August 2017, he was with the Division of Computational Physics, Institute for Computational Science, and the Faculty of Electrical and Electronics Engineering, Ton Duc Thang University, Ho Chi Minh City, Vietnam. Since September 2017, he has been working as a Lecturer at the School of Electronics and Telecommunication, Hanoi University of Science and Technology. He has authored and coauthored over 100 technical journal and conference papers. His research interests include antennas, metamaterials, metasurfaces, metamaterial-based antennas, metasurface-inspired antennas, circularly polarized antennas, and millimeter-wave antennas. He has served as a reviewer for over 15 scientific journals. He has been selected as a Top Reviewer of IEEE Transactions on Antennas and Propagation, in 2020 and 2021.

**CHIEN DAO-NGOC** (Senior Member, IEEE) received the Dipl.Eng. degree from the School of Electronics and Telecommunication (SET), Hanoi University of Science and Technology, Vietnam (HUST), in 1997, and the M.Sc. and Ph.D. degrees from the Department of Electronics and Computer Engineering, Gifu University, Japan, in 2002 and 2005, respectively.

From April 2005 to October 2011, he worked as a Senior Lecturer at SET, HUST, and appointed as the Director of the Centre for Research and Development on Satellite Navigation Technology, South East Asia, in 2009. He has been appointed as an Associate Professor, since November 2010. Since November 2011, he has been with the Department of High Technology, Ministry of Science and Technology, Vietnam, and appointed as an Adjunct Professor at SET, HUST. His research interests include computational electromagnetics based on MoM and FDTD method, analysis and design of modern antenna, and of nanometric integrated optical circuits based on surface plasmon polaritons.

Dr. Dao-Ngoc has been a reviewer for several journals/transactions of Optical Society of America (OSA), IEEE, Elsevier, and American Geophysical Union (AGU) as well as numerous of technical and science conferences.

**NGHIA NGUYEN-TRONG** (Member, IEEE) received the Ph.D. degree in electrical engineering from The University of Adelaide, Adelaide, SA, Australia, in 2017.

He is currently a Lecturer with The University of Adelaide. His main research interests include microwave circuits, advanced materials, absorbers, and various types of antennas.

Dr. Nguyen-Trong was a recipient of the Best Student Paper Award by the 2014 IWAT, the 2015 IEEE MTT-S NEMO, and the 2017 ASA Conferences; and the Best Paper Award by the 2018 and 2020 AMS Conference. He received the Doctoral Research Medal for his Ph.D. degree. He has been continuously selected as a Top Reviewer for IEEE Transactions on Antennas and Propagation, in 2018, 2019, 2020, and 2021, and IEEE Antenna Wireless and Propagation Letters, in 2018 and 2021. He serves as the Technical Co-Chair for the 2020 Australian Microwave Symposium (AMS) and 2022 IEEE International Symposium on Antennas and Propagation. He is listed among Australia's Top 40 Early Career Researchers by The Australian, November 2021.

**KHAC KIEM NGUYEN** (Member, IEEE) was born in Hanoi, Vietnam, in 1978. He received the B.Eng., M.Sc., and Ph.D. degrees from the School of Electronics and Telecommunication (SET), Hanoi University of Science and Technology (HUST), Vietnam, in 2001, 2003, and 2017, respectively. Since 2001, he has been working as a Lecturer at SET, HUST, and a Researcher at the CRD Laboratory, HUST. His research interests include design microstrip antenna for next generation mobile communication systems as well as passive RF components.

• • •